Exit Plane and Suction Surface Flows in an Annular Turbine Cascade with a Skewed Inlet Boundary Layer

Jeffery P. Bindon†

The flow in the exit plane and on the suction surface of an annular turbine cascade was examined experimentally for conditions of inlet boundary layer skewing similar to that found in a real turbine and for the collateral inlet as found in most cascade tests. Skewing was introduced by rotating the nose cone ahead of the cascade.

At the cascade exit, the loss distribution pattern, as measured by a 3 hole cobra probe, showed that the corner vortex at the hub is displaced radially to almost a mid-span position by the skewed inlet boundary layer. This movement was attributed to the stronger endwall crossflows being radially directed as they strike and rise up onto the suction surface. The radial displacement and endwall crossflow effect was also seen in surface flow visualization studies.

The overall cascade loss coefficient and deviation angle are significantly reduced by skewing. Traverses taken on the suction surface confirmed the separated flow effects seen in the flow visualization pictures.

The general conclusion is that skewing plays a significant role in determining the flow phenomena in turbine cascades and that these effects should be borne in mind when interpreting the results taken from plane cascades.

NOTATION

- C velocity
- C_x axial velocity component, free stream inlet velocity
- C_∞ free stream velocity above boundary layer
- C_{pt} total pressure loss coefficient = $(p_0 - p_{01})/\frac{1}{2}\rho C_x^2$
- h_c crossflow height, $h_c C_\infty = \int_0^\delta w \, dy$
- p_0 total pressure
- p static pressure
- ρ air density
- U blade speed, inner annulus surface speed
- W relative velocity
- w boundary layer absolute velocity component normal to free stream direction
- y distance measured normal to surface
- δ boundary layer height
- δ^* boundary layer displacement thickness
- δ_x^* displacement thickness determined using only axial velocity component
- θ boundary layer momentum thickness
- θ_x momentum thickness determined using only axial velocity component
- l refers to cascade inlet

1 INTRODUCTION

The flow patterns at the exit of a cascade are largely determined by pressure gradients within the cascade which tend to drive boundary layer fluid into the suction surface corners to form vortices. The endwall boundary layer forms the most important components of the corner vortex. Starting from the cascade inlet, the endwall layer becomes increasingly skewed towards the suction surface as flow progresses towards the outlet. In most experimental studies of cascade parameters, the endwall boundary layers at inlet have been collateral whereas in real machines the relative motion between blade rows causes the low momentum fluid near the surface to have not only a different direction to the mainflow (i.e., skewed) but also to have a high velocity. As shown in Fig. 1, the mainstream absolute velocity C from a stator combines with the rotor velocity to form the relative velocity W with near zero rotor blade incidence. The low velocities in the boundary layer form high relative velocities at high negative incidence and the effective inlet flow is skewed and very energetic near the surface. The same is true for a stator receiving flow from a rotor but for compressor blading, the relative motion produces positive incidence at inlet and tends to counteract the skewing due to the endwall pressure gradient.

Since the action of the blade to blade pressure gradient is to promote skewing, the fact that the inlet is already skewed in real machines is likely to influence considerably the deductions and measurements which can be made with normal cascades. Previous studies, by Moore and Richardson (1) for a compressor and Carrick (2) for an impulse turbine, have modelled the effect of skewing in plane cascades. This present work, following closely on that of Sjolander (3) and using essentially the same apparatus, seeks to add to the understanding of cascade flow by simulating the boundary layer skewing effect by rotating the hub ahead of an annular turbine cascade. The direction of rotation is towards the suction surface to produce the negative incidence in the boundary layer as shown in Fig. 1. A study dealing with flow phenomena on the endwall itself has already been presented in Bindon (4). A 3 hole cobra probe was used to measure the flow conditions at the cascade exit for the collateral case and for an equivalent blade speed to axial velocity ratio (U/C_x) of unity. A single hole probe was used to explore some of the loss contours on the suction surface and an oil dot and film technique used to show the suction surface flow patterns. An associated work,

† Senior Lecturer, Department of Mechanical Engineering, University of Natal, Durban 4001, South Africa.

Received 24 April 1979 and accepted for publication on 25 January 1980.

0142/727X/80/0600-0057$02.00

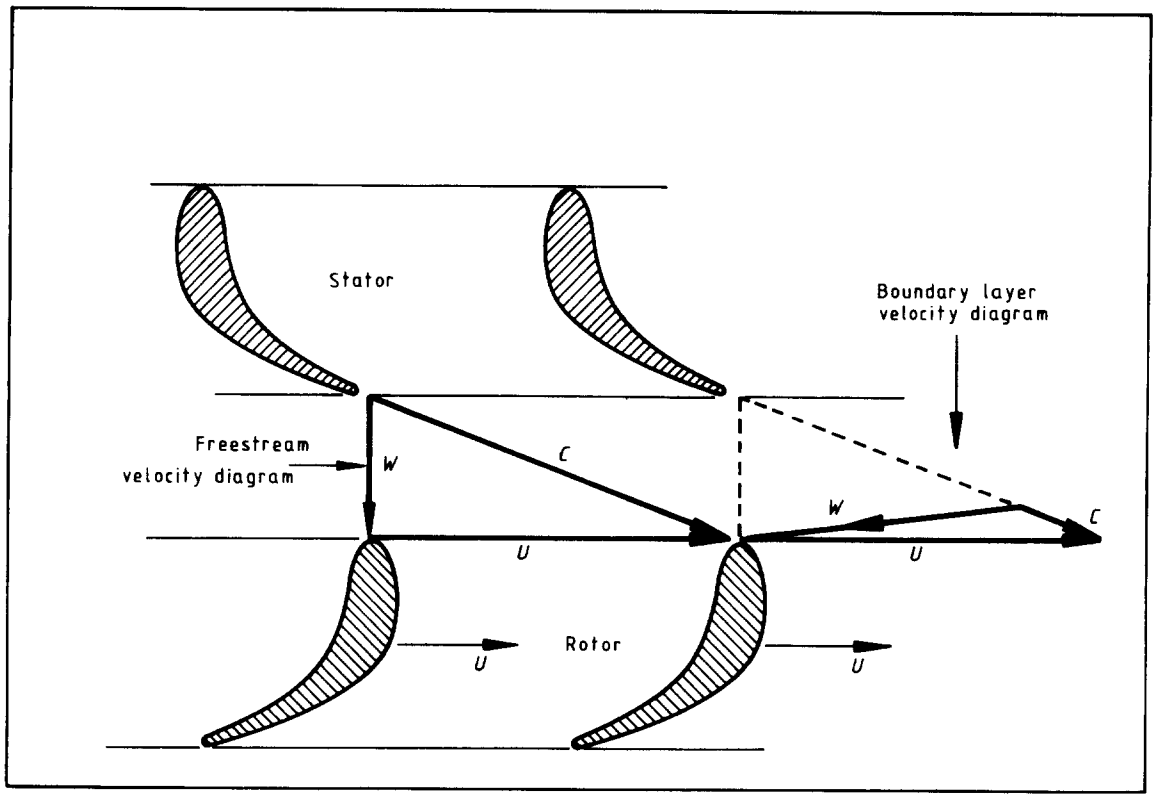

Fig. 1. Velocity and incidence changes in endwall boundary layer

Bindon, et al. (5) in the same apparatus, examined the effects of disc cooling air injection on the endwall and exit flow patterns.

2 PREVIOUS WORK

A number of studies have been made of the flow at the exit of a cascade. Armstrong (6) determined the loss contours and velocity vectors at the outlet from an impulse cascade with a thin and a thick inlet boundary layer. The effect of the thicker inlet boundary layer was to distribute the losses more evenly across the suction corner and to raise the centre of the high loss vortex from 11 per cent to 33 per cent span.

Came (7) studied the outlet loss pattern for six inlet boundary layer thicknesses and for three values of incidence. Although the high loss core does not seem to change with varying boundary layer thickness, it does lift markedly as the incidence increases.

Turner (8), for a planar nozzle cascade, measured the outlet loss distribution for a normal boundary layer and for the inlet boundary layer removed. The two loss patterns are similar showing a more widespread distribution of losses for the thick boundary layer but no change in the location of the high loss core. Carbon black flow visualization indicates strong cross flows and a streak on the suction surface was said to mark the path of the fluid swept off the endwall and rolled up into a vortex.

Herzig et al. (9) conducted extensive flow visualization and downstream traverse studies in planar and annular compressor cascades. Smoke traces indicate the movement of low energy fluid towards the suction surface and of its roll up into the corner vortex. Higher losses were seen in the hub corner vortex and are attributed to the radial pressure gradient moving low energy fluid towards the hub and down the suction surfaces and into the blade wakes.

The first to recognize and account for the skewing of the inlet boundary layer were Moore and Richardson (1) who simulated the effects of relative motion by a transverse jet blowing along the endwall upstream of a compressor cascade and out through a hole on the opposite side. No measurements were taken of the exit plane loss patterns but endwall traverses indicated that by mid chord the pressure gradients had neutralized the inlet skewing.

Sjolander (3), working in an annular turbine cascade, measured the outlet loss contours and the boundary layer profiles in the endwall and using surface flow visualization techniques has generated detailed data and some factors relating the endwall, the suction surface, and the downstream observations.

Langston et al. (10) used a large scale plane cascade of 70 degrees turning and a 5 hole cobra probe to provide 3D loss patterns within the cascade as well as downstream, the probe also providing some data on radial velocity components.

Carrick (2) studied the effect of skewing on a high turning angle impulse cascade by arranging a moving belt upstream of the blades. The effects of skewing were to increase the overall loss coefficient and slightly lift the position of the high loss peak in the suction corner away from the endwall.

3 APPARATUS AND EXPERIMENTAL TECHNIQUE

The annular cascade is fully described in Sjolander (3) and the adaptions to allow the inlet nose cone to rotate in Bindon (4). Figure 2 presents a cross section through the adapted tunnel and Table 1 summarizes the cascade geometric data.

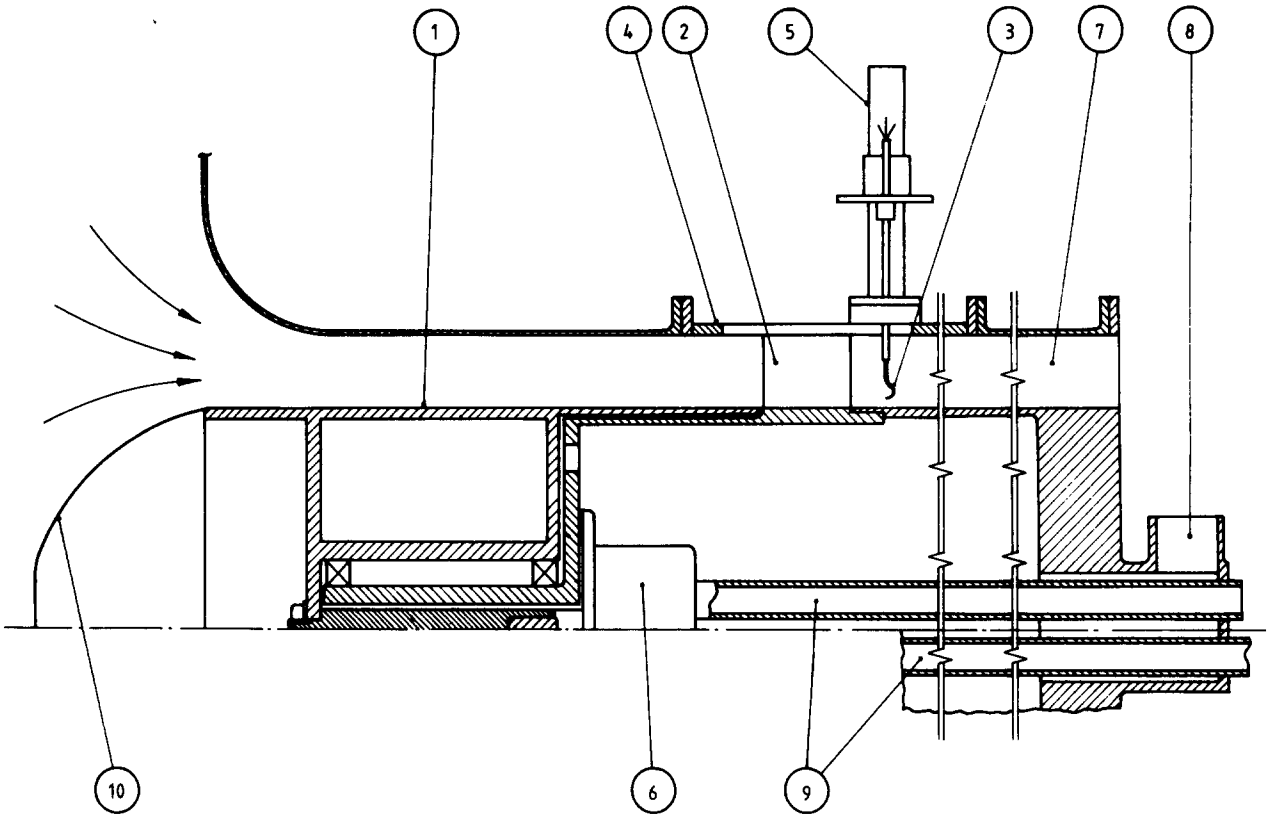

Fig. 2. Section through annular cascade wind tunnel with upstream rotating hub

1. Rotating nose cone
2. Cascade
3. 3 hole goose neck cobra probe
4. Plexiglass outer annulus
5. Traverse gear
6. Air motor
7. Straightening vane
8. Transverse injection inlet
9. Compressed air hoses
10. Dish

A 3 hole 90 degree cobra probe, head dimensions 1·99 mm × 0·64 mm with 0·08 mm bores was used to traverse the inlet boundary layers and the flow in the exit plane. Since a 3 hole probe cannot be calibrated for velocity vectors normal to the plane of the probe, the effect of such flows on the pressures measured is not known. Although radial flows are not significant in the inlet boundary layers, they are at the outlet, particularly in the region of the corner vortex. The inaccuracies are likely to be greater for the yaw angle and static pressure than for the total pressure which is of more importance in this paper. The inaccuracies would also probably be less than the errors associated with probing in flow with sharp velocity gradients where the two sides of the probe experience different conditions.

The shank of the cobra probe was shaped as a

Table 1

Annular cascade geometric and flow data

Profile	T6
Camber line	parabolic, maximum at 40%
Thickness	15% at 40% chord
Chord	76·2 mm (3 in)
Stagger angle	34°
Camber angle, blade leaving angle	50° (constant)
Gas inlet angle	0° (constant)
Gas leaving angle (approx.)	45°
Pitch chord ratio	0·785 (at hub)
Hub diameter	304·8 mm (12 in)
Blade span	50·8 mm (2 in)
Axial velocity at inlet	42 m/s ($R_N = 2 \times 10^5$)

flattened question mark to minimize interference and the tip was located at the centre of rotation and could be yawed without positional change. The probe was mounted in a United Sensor traversing gear adapted to include a geared potentiometer for yaw angle, a dial gauge for height indication and electric contact indicator to determine zero height when the probe touched the surface. The probe was positioned circumferentially by rotating the whole inner annulus and cascade with respect to the outer annulus.

The pressures were measured on a single Rosemount 831A3 differential pressure transducer, the connections allowing side hole nulling as well as all pressures to be read with respect to upstream static. Pressure lines contained two cotton wool dampers in series to reduce fluctuations. The dampers could be short circuited to reduce response time when switching.

A 3 hole cobra probe can be used without nulling. The yaw angle is held constant and the three pressures recorded and converted into true yaw angle, total and static pressures via calibration curves as in Sjolander (3). Although it is accurate and rapid, it does not provide a direct reading of total pressure and yaw angle to the experimenter and this is needful in an exploratory study where the limits and nature of a boundary layer are not known. To work in the nulling mode is time consuming. In this study a 'semi-nulling' mode was used in which the probe was approximately and rapidly nulled without using the oscillation dampers and without striving for precision. This brought the probe comfortably into the range where the centre hole read a true total pressure and the yaw angle required only a minor correction via a calibration as in Sjolander (3) using the actual values of side hole pressure. The probe calibration was done at a reference point 2·54 cm upstream of the leading edges, mid height and at a mid-pitch position between two blade leading edges. The flow angle here was assumed zero.

Visualization of the suction surface flow was achieved by applying a thin film of titanium dioxide mixed with oil as described by Sjolander (3).

4 INLET BOUNDARY LAYERS

The inlet boundary layers for the two cases examined, collateral ($U/C_x = 0$) and skewed ($U/C_x = 1$) were measured 2·54 cm (or 40 per cent axial chord) upstream of the leading edges and at a mid-pitch position to minimize the possibility of the flow already deflecting due to the blades. The boundary layer profiles are given in Fig. 3 where some integrated parameters are included.

These boundary layer profiles are important in that they constitute the basis of comparison between the collateral case and the skewed cases. Ideally the two boundary layers should be chosen so that the effect of skewing alone is modelled without other variables confusing the results. In the apparatus used it was not possible to exercise any control over the naturally resulting boundary layers and thus some doubt will exist as to whether the effects are due to skewing alone.

As seen in Fig. 3, the skewed boundary layer is thicker than the collateral one, a thickening which is probably due to the swirling flow near the surface being centrifuged in a main flow which has no radial pressure gradient. The same thickening was reported by Steinheuer (11) for a similar geometry and for identical velocity ratios. For comparison, these results are included in Fig. 3 and they are seen to be much thinner than in the present study. This could be due to differences in the shape of the nose cone.

Boundary layer parameters

U/C_x	δ^*	δ^*_x	θ	θ_x	h_c	C_{pt}	δ^*/θ	δ^*_x/θ_x
0	0·958	0·958	0·704	0·704	0	-0·0506	1·36	1·36
1	1·094	1·418	0·891	1·024	1·782	-0·0595	1·23	1·38
Ref. 7	0·61	0·61	0·35	0·35	0	-	1·74	1·74

(thickness, mm)

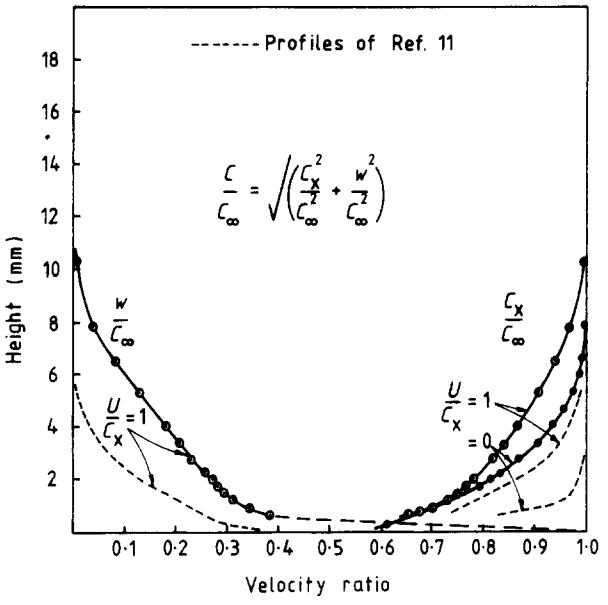

Fig. 3. Inlet boundary layer profiles

Although the thicker skewed boundary layers are not ideal, it should be pointed out that it will not be a simple matter to decide which parameters should and could be controlled and an even more difficult task to achieve the desired profiles experimentally. Fortuitously, certain parameters, although not identical, are similar in magnitude. These are displacement and momentum thickness taken in the absolute velocity plane and the total pressure coefficient (or kinetic energy deficit).

The crossflow height h_c of Fig. 3 is defined as that height of mainstream flow turned to flow normal to the mainstream direction. For incompressible flow

$$C_\infty h_c = \int_0^\delta w \, dy$$

5 EXIT PLANE LOSS CONTOURS

The flow at 25 per cent axial chord downstream of the cascade was traversed up to a height of 70 per cent span (36 mm) above the inner endwall. The resulting two-dimensional loss patterns are given as contours of total pressure loss coefficient in Fig. 4 for the collateral case and in Fig. 5 for the skewed case. The zero point on the tangential distance axis is the wake peak at mid span and 25 per cent chord downstream for the unskewed case.

The results are generally similar to those found by previous workers as for example references 6–8 and very similar to the result in Sjolander (3) for essentially the

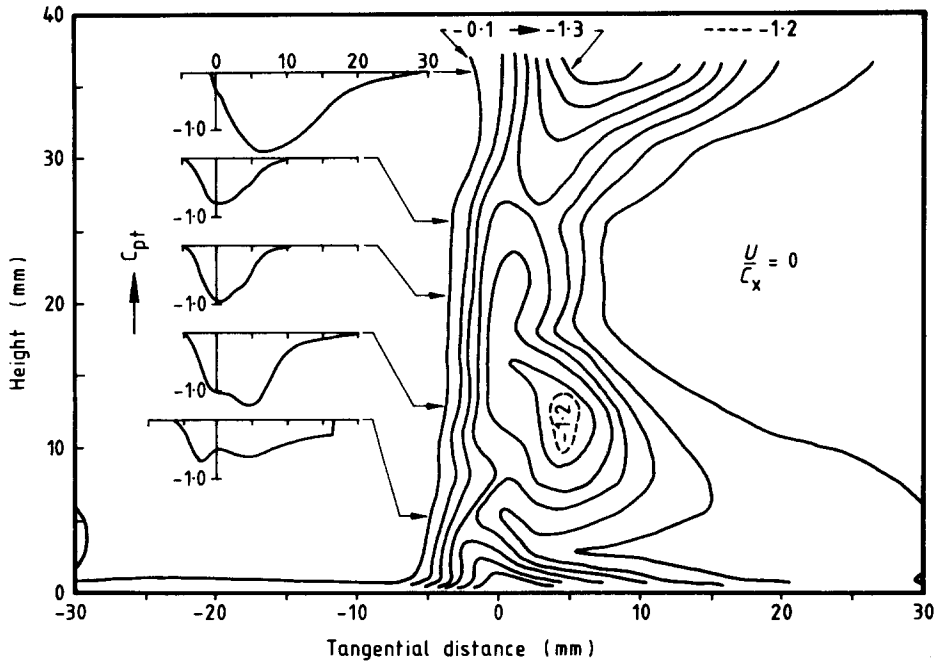

Fig. 4. Pressure loss contours and tangential traverses, cascade exit, unskewed inlet

same apparatus. The loss distribution clearly shows the blade wake in the vertically running lines closely spaced on the pressure side, the hub and tip corner vortices as zones of high loss, and a small area of high loss beneath the vortex and close to the surface.

When Fig. 4 is compared with the similar result in Sjolander (3) for a much thinner collateral inlet boundary layer, the effect of inlet boundary thickness can be commented on. The two results are very similar, the passage vortex being at the same height and the losses slightly more spread out as reported by Turner (8).

The effect of skewing the inlet boundary layer is seen to raise the passage vortex significantly and introduce a large amount of low loss fluid into the area beneath the vortex. The raising of the vortex also appears to have squeezed the suction surface boundary layer into a smaller area and consequently the mid-span wake is much thicker. The raising of the passage vortex is discussed again when the suction surface flow visualization is dealt with but it appears to be caused by the much higher levels of crossflow kinetic energy carrying the rolled up inlet boundary layer much further up the suction surface. Traverses done at a higher equivalent blade speed, $U/C_x = 2$, in Bindon (4), showed that increased skewing will lift the vortex even further.

Since traverses were conducted to a much greater height from the endwall than in Sjolander (3), the upper or tip passage vortex is encountered and in general is not symmetrical with the lower vortex. In both cases the tip loss contours and vortex do not appear to be greatly

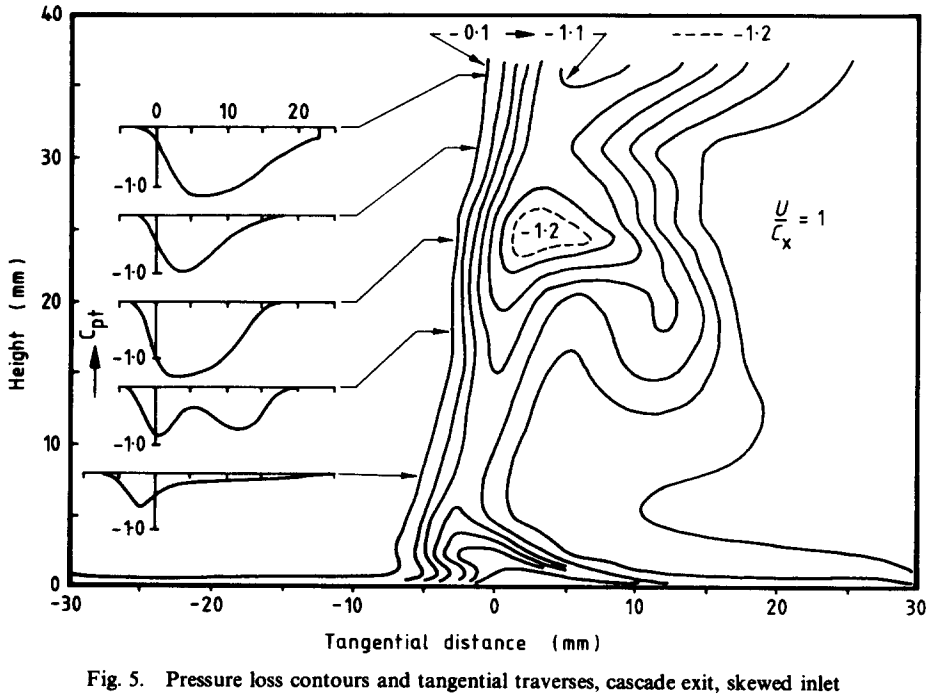

Fig. 5. Pressure loss contours and tangential traverses, cascade exit, skewed inlet

influenced by inlet skewing. The asymmetry could be due to the losses being greater over the tip half or due to the low velocity fluid being moved towards the hub by the radial pressure gradient. The blades did not seal against the outer annulus and leakage could increase the losses towards the tip.

The vortex seems to lift away from the hub as it progresses across the suction surface and towards the downstream traverse point. This is somewhat unexpected since the radial pressure gradient would tend to drive it downwards. It would seem that the crossflow components, directed radially by the suction surface, are responsible for the lifting.

The small zone of high loss fluid beneath the corner vortex and close to the endwall surface in the suction corner has been associated, in references 4 and 3, with a strong separation line seen in the endwall flow visualization patterns. These photographs are reproduced here in Figs. 7 and 8, interpreted in Fig. 9 and discussed in Section 7 below. The loss contours show clearly the high loss zones but due to the choice of tangential axis zero (wake peak at mid span for the unskewed case at traverse point 19 mm downstream of trailing edge) the exact correspondence of position cannot be determined with certainty.

6 AVERAGED DOWNSTREAM FLOW PARAMETERS

The flow at the cascade exit can be integrated to give circumferentially averaged variations of loss (excluding inlet boundary layer) and gas leaving angle with radius as well as the overall loss coefficient and deviation angle.

	$\frac{U}{C_x}$	Deviation		Hub half mass averaged overall loss coeff.	Hub half inlet loss coeff.
		Mid span	Avr.		
•	0	5·91	5·04	- 0·1131	- 0·0506
•	1	7·52	3·68	- 0·0861	- 0·0595

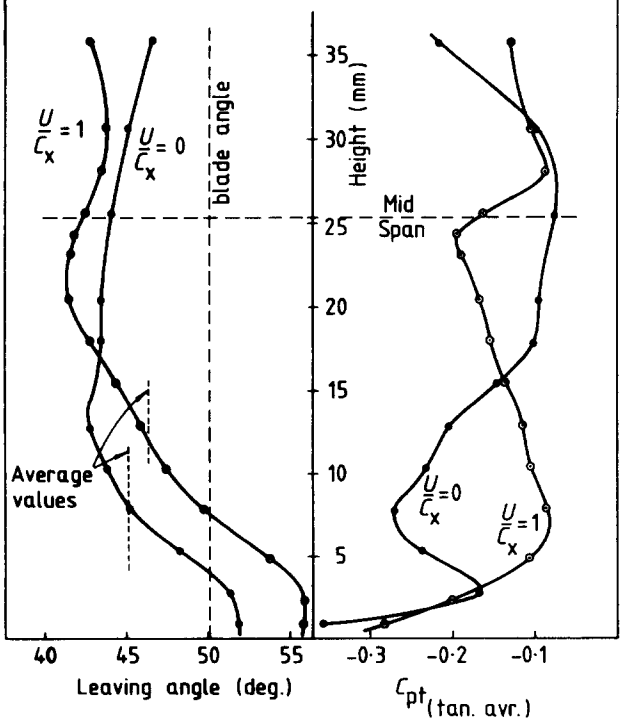

Fig. 6. Tangentially averaged leaving angle and loss coefficient (excluding inlet boundary layer) at cascade exit

This is done in Fig. 6 where the quantities shown are for the hub half only since the traverses were not completed up to the outer radius.

As would be expected, the crossflow increases the leaving angle near the hub and skewing makes this increase 4 degrees larger. The mid span leaving angle, which is what is normally taken as the leaving angle for the cascade, is seen to be a good approximation for the unskewed case but in the skewed case overturning at the hub and underturning at mid span produces a 4 degree discrepancy. This would indicate that skewing, at least for low aspect ratio blades, invalidates the planar cascade collateral models normally used for deviation angle prediction.

The loss variation with height shows the vortex for the unskewed case but no such distinct peak for the skewed case. Above mid span for the skewed case, a sharp drop in the loss coefficient is seen over a small region of flow between the tip vortex core and the squeezed up suction surface layer. The most notable result here is the reduction in overall loss coefficient due to skewing from 0·113 to 0·086 (or 24 per cent), a figure which is accompanied by a 1 degree greater fluid deflection.

7 SUCTION SURFACE FLOW VISUALIZATION

The flow on the suction surface is of particular interest since it carries the flow off the endwall and forms the passage vortex. In comparison, flow visualization on the pressure surface shows only flow parallel to the endwall with no peculiarities. The flow patterns observed are shown in Figs. 7 and 8 for the skewed and unskewed

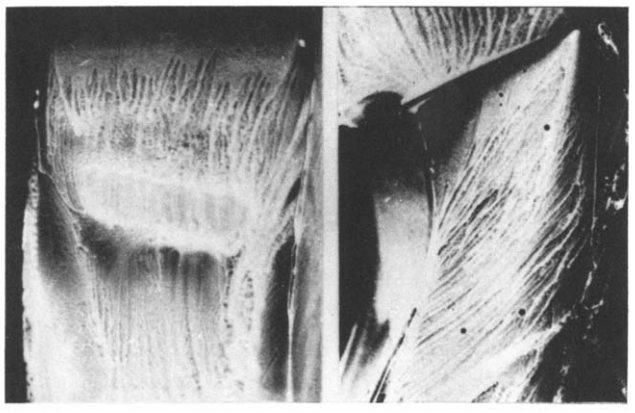

Fig. 7. Folded down suction surface and endwall flow visualization with stationary upstream endwall ($U/C_x = 0$)

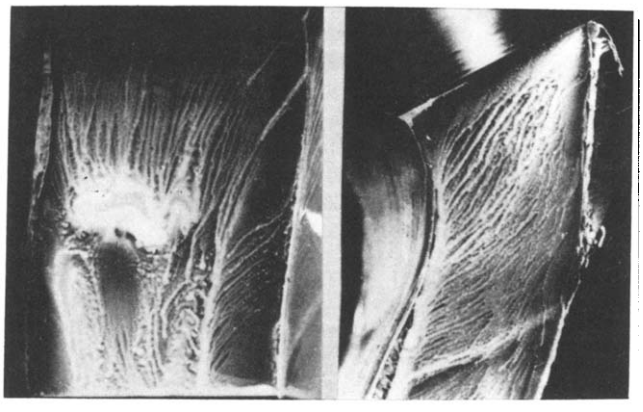

Fig. 8. Folded down suction surface and endwall flow visualization with moving upstream endwall ($U/C_x = 1$)

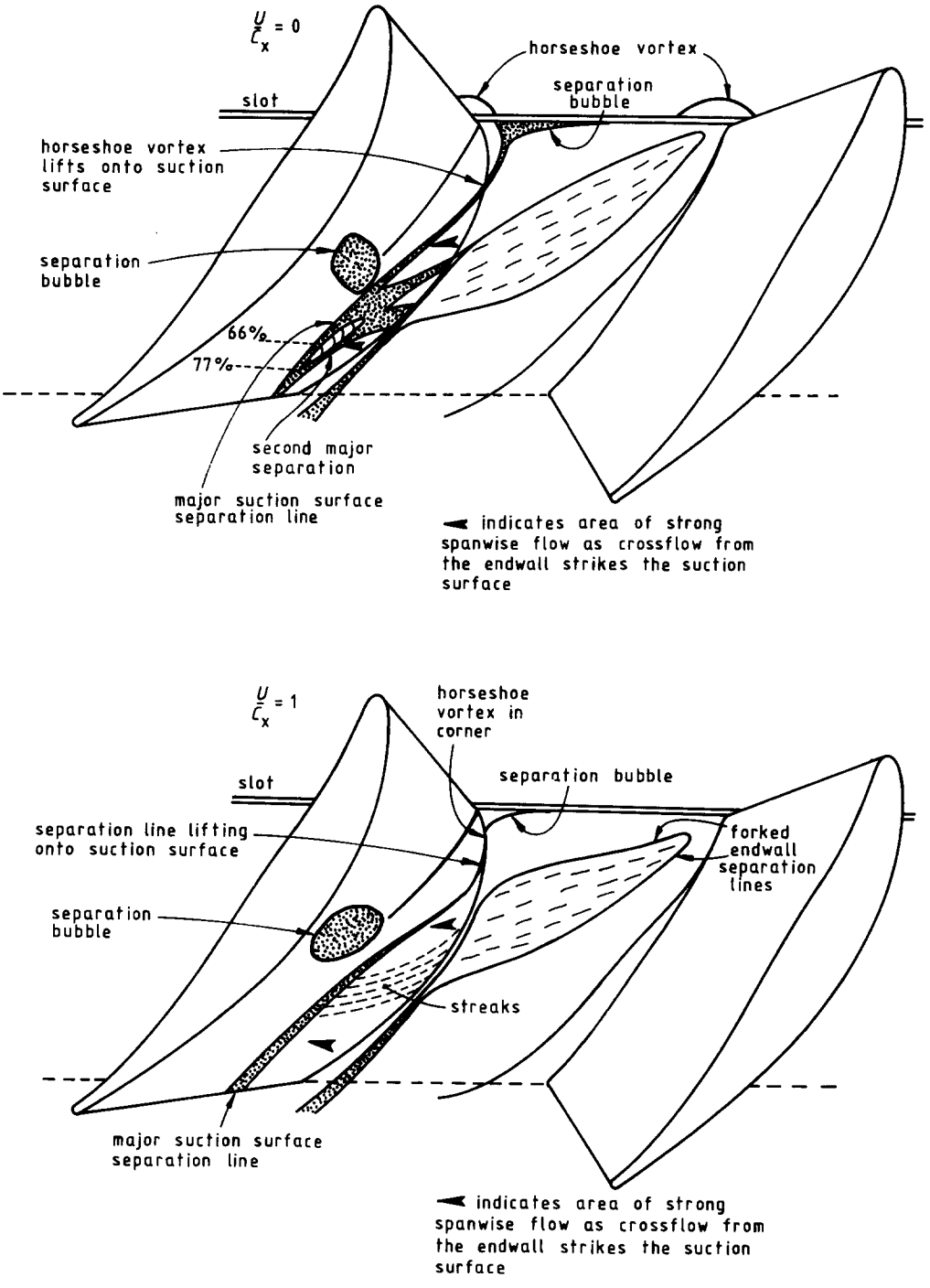

Fig. 9. Suction surface and endwall flow visualization interpretation

case, respectively. Also reproduced are the endwall surface flow patterns which have been fully discussed in references 4 and 3. For clarity and for correspondence with an interpretive sketch of the major flow phenomena on the two surfaces given in Fig. 9, the suction surfaces are shown as folded down from their normal vertical position.

As in Sjolander's (3) study, the flow appears to have a laminar separation bubble at about mid chord. This separation bubble seems generally larger than that found by Sjolander. The surface flow has also clear separation lines which appear to be linked to the lines on the endwall. In both the skewed and unskewed cases, a major separation line is seen moving towards the trailing edge, the height of which seems to indicate that these lines are associated with the passage vortex seen in the endwall traverses at 95 per cent chord (see reference 4). The origin of these separation lines seems to lie in the suction side horseshoe vortex leg on the endwall near the leading edge. In the unskewed case this can be seen to cross and continue with the slot separation bubble near the suction surface leading edge, move into the suction surface corner, and lift out onto the suction surface at about 25 per cent axial chord. In the skewed case the horseshoe vortex on the endwall cannot be seen but if present it would appear that skewing has pushed it near to the leading edge so that after traversing the slot it moves downstream right in the suction surface corner.

There is then a particularly clear separation line lifting onto the suction surface and forming the major separation line. The above arguments regarding the horseshoe vortex and the suction surface separation line cannot be regarded as conclusive since the flow is complex and the flow visualization technique has insufficient resolution.

The major suction surface separation line and the corner vortex associated with it is clearly joined by fluid from the endwall as evidenced by the strong spanwise flows seen coming off the endwall and ending in the separation line. This vertical flow contains lines which seem to be connected to the trails of the forked endwall lines originating near the pressure surface leading edge. In the skewed case, a patch of vertical flow seems to leave streaks and this patch seems to correspond with the patch between the forked endwall lines. In the unskewed case these streaks are very strong separation lines and seem to form a second major separation line beneath the first one. This double separation line is discussed again below when suction surface traverse data is dealt with.

The flow above the major separation line is dominated by the laminar separation bubble and the reattached flow behind it. This bubble seems more extensive than in the skewed case and this reduction in size is caused by a larger portion of the suction surface flow being controlled by the flow from the endwall. The suction surface boundary layer could partially wrap up into the passage vortex due to the radial pressure gradient but probably considerable concentration of the boun-

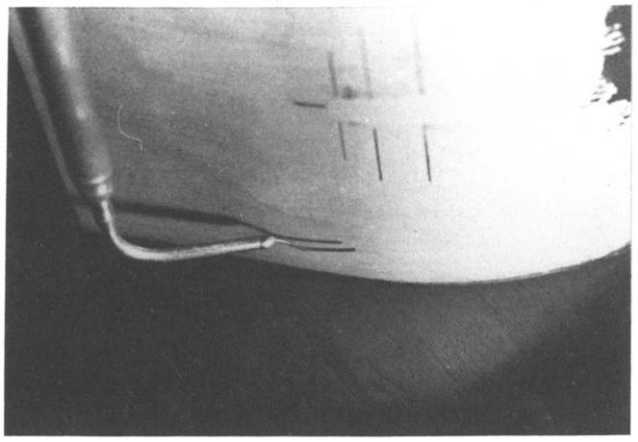

Fig. 10. Single hole total pressure probe used for traversing suction surface flows

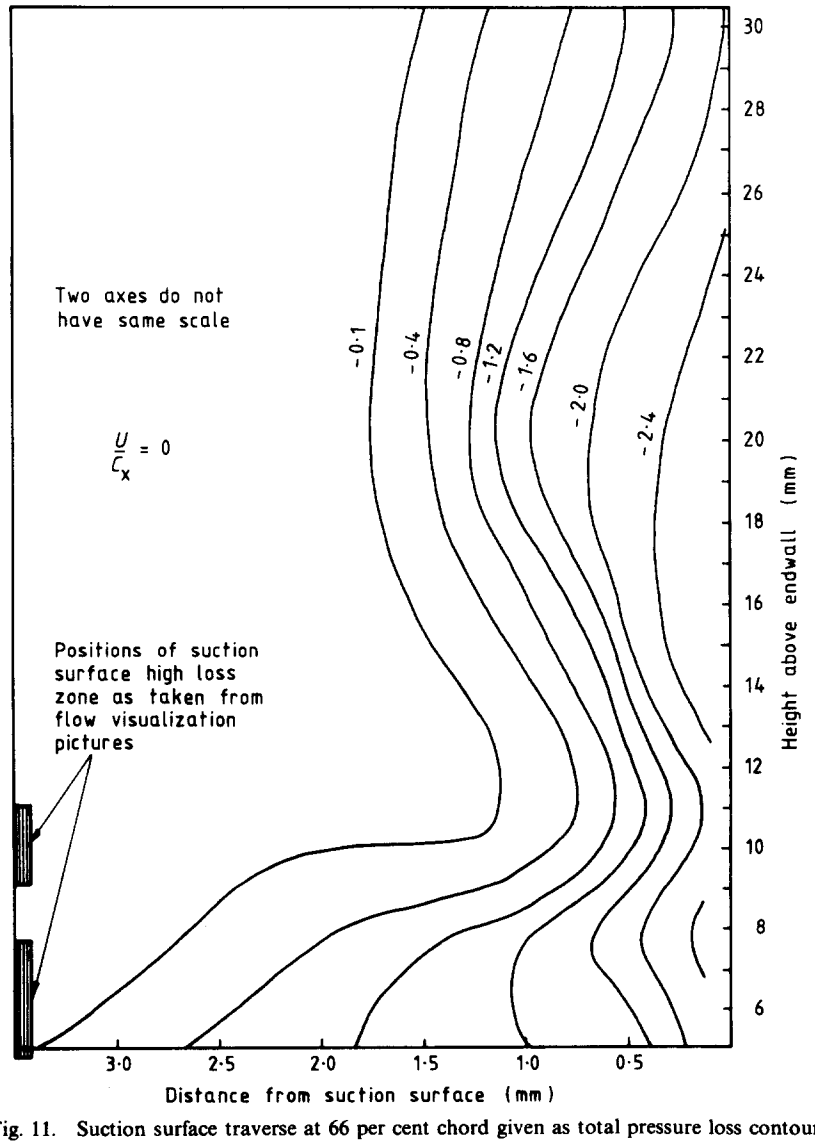

Fig. 11. Suction surface traverse at 66 per cent chord given as total pressure loss contours

dary layer takes place. This is thought to give rise to the peak outlet loss occurring in the trailing edge wake at mid span rather than in the passage vortex as in the unskewed case.

8 SUCTION SURFACE TRAVERSES

In an attempt to understand the suction surface flow, a limited number of traverses were taken with single hole 0·4 mm outer diameter total pressure probe aligned parallel to the suction surface and endwall. The probe was mounted in the traversing gear and the distance from the suction surface determined by rotating the yawmeter, the probe tip then moving in an arc. The point of contact with the blade surface was electrically determined by painting the blade surface with conducting paint. The probe and suction surface are shown in Fig. 10.

Traverses were done in two planes for the unskewed case only to examine the major separation lines seen on the suction surface and thought to be associated with the corner vortex and, as argued in the previous section, with separated flow patterns coming off the endwall. Figure 7 indicates that two major separation lines exist at about 66 per cent chord whereas at 77 per cent, the upper line has merged downward with the lower line. Traverses at 66 per cent, shown as loss contours in Fig. 11 confirm the flow visualization pictures and two high loss zones were detected but with considerable discrepancy in the position of the upper line. The result further downstream at 77 per cent chord, Fig. 12, shows values as high as in the previous traverses but only a single high loss zone is seen somewhere in between the two previous ones.

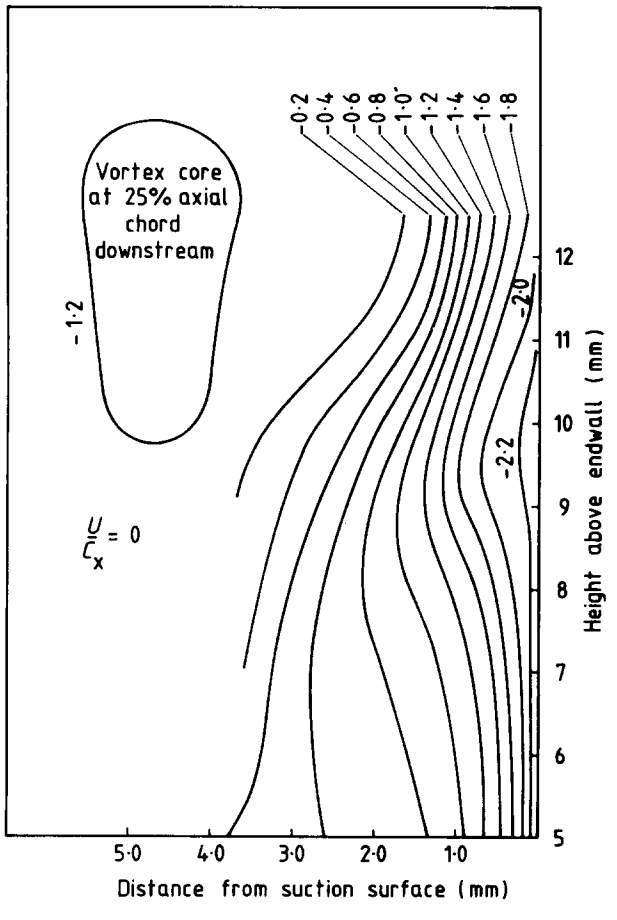

Fig. 12. Suction surface traverse at 77 per cent chord given as total pressure loss contours

9 CONCLUSIONS, RECOMMENDATIONS, AND ACKNOWLEDGEMENTS

The effects of skewing as modelled in this study were generally found to be significant but consideration should be given to the type of flow and the type of apparatus which will more realistically model the kind of skewed boundary layer occurring in a real turbomachine.

Downstream of the cascade, loss and angle data showed that the passage vortex is lifted away from the endwall with skewing, and that deflection angle is increased with skewing. Over the collateral case, the overall loss coefficient was reduced by 25 per cent for the low speed skewed case which poses a question on the validity of plane cascade secondary loss correlations and which invites further study.

Suction surface flow visualization revealed that endwall crossflow moves radially along the suction surface when it leaves the endwall. These radial flows are much stronger with skewing even to the extent of raising the passage vortex and squeezing the boundary layer flow on the suction surface.

The complexity of the flows examined has led to some difficulty in interpreting the link between surface phenomena as revealed by flow visualization and the data obtained by traversing the boundary layers. More detailed traverse data is needed as well as flow visualization methods better able to resolve the different flows.

The present work was restricted to a fixed aspect ratio, blade geometry, incidence angle, and to a turbine cascade configuration. Although some of the results will probably be less marked when changes are made, these parameters should be varied in future work. Finally, since all studies have shown the very great change in boundary layer thickness between pressure and suction surface at cascade exit, the periodic nature of the inlet layer as well as its skewed nature should be examined.

The author would like to acknowledge the meticulous work by Sjolander which made the present work possible, the hospitality of the Carleton University Mechanical and Aeronautical Department and Iowa State University Mechanical Engineering Department where, respectively, experimental and analytical work were done, the funding supplied by the National Research Council of Canada, the South African Council for Scientific and Industrial Research, and the University of Natal and the craftsmanship of John Batky who made the rotating hub for the wind tunnel.

REFERENCES

(1) MOORE, R. W. and RICHARDSON, D. L. 'Skewed boundary layer flow near the endwalls of a compressor cascade', *Trans. ASME* 1957, **79**, 1789

(2) CARRICK, H. B. 'Secondary flow and losses in turbine cascade with inlet skew'. *Agardograph* CP214, 1977, (3), paper 9-1

(3) SJOLANDER, S. A. 'The endwall boundary layer in an annular cascade of turbine nozzle guide vanes', Technical Report No. ME/A 75-4, Carleton University, 1975

(4) BINDON, J. P. 'The effect of hub inlet boundary layer skewing on the endwall shear flow in an annular turbine cascade', *A.S.M.E.* paper No. 79-GT-17
(5) BINDON, J. P., ABURWIN, B. A., and MACCALLUM, N. R. L. 'Comparison of transverse injection effects in straight and in annular cascades', *A.S.M.E.* paper No. 79-GT-13
(6) ARMSTRONG, W. D. 'The secondary flow in a cascade of turbine blades', *A.R.C. Rep. and Mem.* No. 2979, 1955, (3)
(7) CAME, P. M. 'Secondary loss measurements in a cascade of turbine blades', *Inst. Mech. Engrs*, Conference Publication 3, 1973, 75
(8) TURNER, J. T. 'An investigation of the endwall boundary layer of a turbine nozzle cascade', *Trans. ASME*, 1957, **79**, 1801
(9) HERZIG, H. Z., HANSEN, A. G., and COSTELLO, G. R. 'A visualization study of secondary flows in cascades', *N.A.C.A.* Rep. 1163, 1953
(10) LANGSTON, L. S., NICE, M. L., and HOOPER, R. M. 'Three dimensional flow within a turbine cascade passage', *ASME*, Gas Turbine Conference paper 76-GT-50
(11) STEINHEUER, J. 'Three dimensional boundary layers on rotating bodies and in corners', Recent developments in boundary layer research, *Agardograph* 97, Part II, 1965, (5), 592